Available online at www.sciencedirect.com
SCIENCE DIRECT®
Journal of Sound and Vibration 271 (2004) 863–882
JOURNAL OF SOUND AND VIBRATION
www.elsevier.com/locate/jsvi

A study of power flow in a coupled plate–cylindrical shell system

Z.H. Wang, J.T. Xing*, W.G. Price

School of Engineering Sciences, Ship Science, University of Southampton, Southampton SO17 1BJ, UK

Received 28 May 2002; accepted 10 March 2003

Abstract

A substructure approach is formulated to investigate the power flow characteristics of a plate–cylindrical shell system subject to both conservative and dissipative coupling conditions. The system is divided into a shell substructure and a plate substructure. The theoretical receptance function of each substructure with a free–free interface condition is formulated by modal analysis to describe the dynamical behaviour of each substructure. The displacement components induced by external forces and the interface coupling forces are deduced, permitting determination of the coupling forces and power flow through the interface between the two substructures. On the basis of the dynamic information of the two substructures and through a synthesis analysis using the geometrical compatibility and force balance conditions on the coupling interfaces, the dynamic characteristics of power flow excited and transmitted within the system are calculated. A power flow density vector and the corresponding energy flow line are defined for this coupled system. The numerical example demonstrates the applicability of the proposed method and illustrates the power flow characteristics associated with the complex coupled plate–cylindrical shell system.

1. Introduction

A power flow analysis (PFA) provides a technique able to model mathematically the medium- to high-frequency responses of structures. The fundamental concepts of power flow analysis, as discussed and described by Goyder and White [1–3], use the rate of energy flow to characterize the dynamic response of vibrating systems. Considerable attention has been focused on the dynamic and power flow behaviour of coupled beams or plate structures adopting different theoretical methods involving mobility, direct dynamic stiffness, travelling and scattering wave receptance theories [4–12].

*Corresponding author. Tel.: +44-23-8059-6459; fax: +44-23-8059-3299.
E-mail address: j.t.xing@ship.soton.ac.uk (J.T. Xing).

0022-460X/$ - see front matter © 2003 Published by Elsevier Ltd.
doi:10.1016/S0022-460X(03)00757-0

Applications of finite element analysis (FEA) to energy flow modelling usually adopt a global model performed on a global system [13–17] or in the case of receptance theory to a local FEA domain [18,19]. Hambric [20] and Gavric and Pavic [21] use FEA to calculate structural intensities. The FEA method applied to a power flow analysis and/or used to perform structural intensity calculations can conveniently model complex structures subject to complex boundary conditions, demonstrating its advantageous applicability. However, in general, because the structural intensity prediction requires an accurate description of various spatial derivatives, it is necessary to admit a large number of modes into the analysis to ensure convergence of solution. This numerical scheme of study, adopting modal superposition, encounters difficulties due to the computational effort required. To ease this problem, Wang et al. [22] proposed a substructure method to analyze the power flow in L-shaped plates. The concept of an energy flow density vector developed by Xing and Price [23] was further investigated and the magnitude and direction of the power flow density vector at any location of the structure were calculated [22,24]. This method provides a way of determining the dominant paths of energy flow using a vector field analysis approach [24].

Many engineering structures are constructed by combinations of plates and cylindrical shells. They are joined together by welds, bolts or dashpots. The coupling between these components may be conservative or compliant and dissipative. In a study of the dynamic characteristics of cylindrical shells, Franken [25] derived the input impedance of a simply supported cylindrical shell but the analysis did not include the influence of bending stiffness of the shell and therefore it has limitations in the estimation of input power in practical applications. Heckl [26] and Fuller [27] derived analytical expressions to evaluate the input radial mobility of an infinite elastic cylindrical shell. Harari [28] developed a general formula to evaluate the transmitted loss of energy or power based on the structural impedance of finite and semi-infinite cylindrical shells. Ming et al. [29] present the mobility function and power flow of a semi-infinite cylindrical shell and two coupled shells using Flugge's shell theory [30,31].

The dynamical characteristics of a coupled plate–cylindrical shell system were discussed by Peterson and Boyd [32] who developed an analytical model for the free vibration of a cylindrical shell with an internal floor using the Rayleigh–Ritz technique. Langley [33] studied the free vibration of a simply supported stiffened cylindrical shell with an internal plate by a dynamic stiffness method. Missaoui et al. [34] investigated the free and forced vibrations of a cylindrical shell with a floor partition based on a variational formulation in which the structural coupling is simulated using artificial spring systems. Missaoui and Cheng [35], Li et al. [36] present findings on the structural acoustic coupling characteristics of a cylindrical shell with an internal floor partition using artificial stiffness to describe the structural coupling between the shell and the plate.

This paper describes further developments of the substructure approach [22] to examine the power flow characteristics in a more complex coupled plate–cylindrical shell system excited by an external force as shown in Fig. 1. The mathematical model adopts a receptance theory [19,37] approach to describe a conservative or compliant and dissipative coupling condition. Thin shell differential equations are used [30,38] to calculate the receptance function of simply supported cylindrical shells subject to different types of excitation using modal analysis theory. The displacement components induced by external forces and the interface coupling forces are deduced, permitting determination of the coupling forces and power flow between the interfaces of the substructures by satisfying geometrical compatibility conditions and force balance

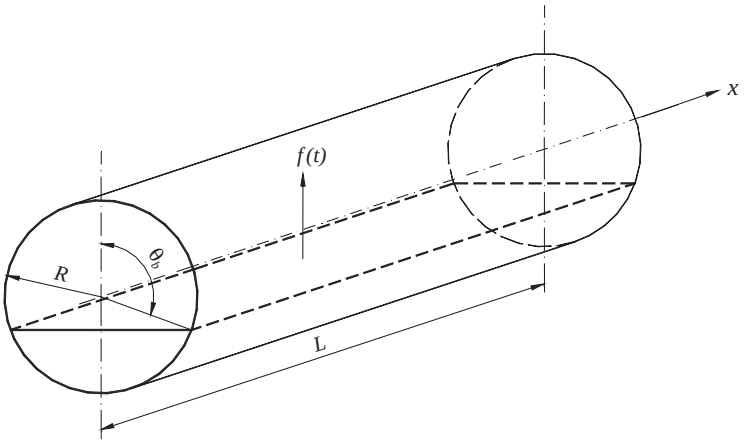

Fig. 1. Schematic illustration of a plate–cylindrical shell system.

equations at the coupling edges. The power flow characteristics in the system and across the coupling edges of the cylindrical shell and plate are calculated for both conservative and dissipative coupling conditions. The substructure approach presented herein divides the large global structure into many small substructures for which dynamic response results are obtained by analytical methods or FEA approaches, thus introducing a higher computational efficiency at the substructure level. Based on these substructure results, the global vibration information of the global structure can be synthesized. When a substructure is readily defined by an analytical solution, a theoretical substructure model is adopted. The main advantage of using a theoretical model in a power flow analysis allows calculation of high-frequency components easily and efficiently, so it is suitable to calculate the detailed distribution of the power flow density vector in the structure. For a system with complex boundary conditions, there are no theoretical natural modes available. It is then necessary to resort to FEA models at the substructure level to derive the vibration modes of each substructure and then by a synthesis process to determine the vibration information of the global system.

In this paper, because of the availability of analytical results, a theoretical model is used. The global shell–plate system is divided into two substructures. That is, a shell substructure and a plate substructure. Section 2 provides the governing equations describing the dynamics of the two substructures together with their theoretical solutions dependent on the two different coupling conditions adopted on the coupling interfaces of the shell and the plate. Section 3.1 develops the necessary power flow analysis formulations defined for this complex shell–plate coupling system. Section 3.2 presents an example calculation to demonstrate the applicability of the developed method through descriptions of power flow characteristics and energy flow transmission paths associated with the complex shell–plate coupling system.

2. Substructure approach to a plate-cylindrical shell system

The plate–cylindrical shell system under investigation is illustrated in Fig. 1. It is assumed that simply supported boundary conditions apply to the ends of the plate and cylindrical shell. This

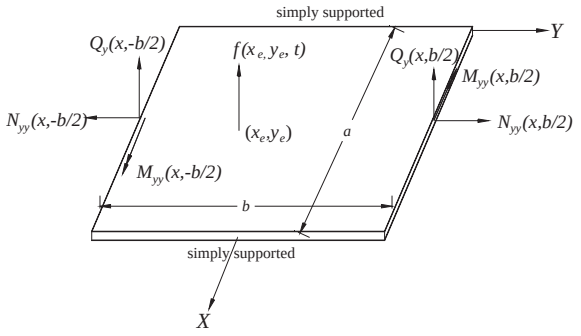

Fig. 2. Schematic illustration of the plate in the local co-ordinate system.

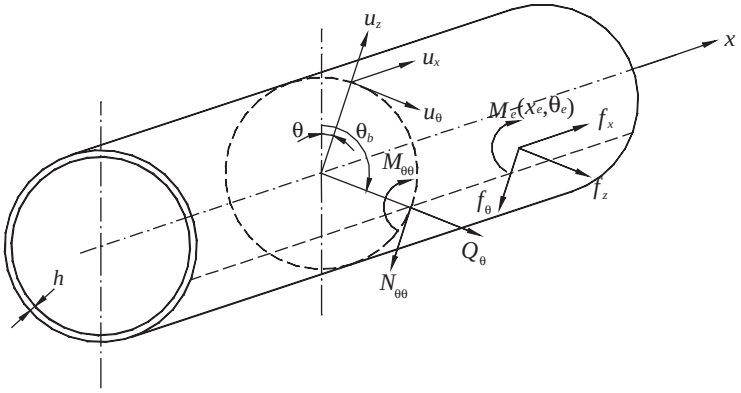

Fig. 3. Schematic illustration of the cylindrical shell in the local co-ordinate system.

total system can be separated into two subsystems. That is, a rectangular plate with simply supported boundary conditions applied to two opposite edges with the coupling edges ($y = \pm b/2$) assumed free and a cylindrical shell with simply supported boundary conditions applied to the two ends of the shell with the two coupling edges ($\theta = \theta_{b1}, \theta = \theta_{b2}$) assumed free.

Each substructure is treated as an independent system but two kinds of forces act on it. One is the external excitation force whereas the other is the internal distributed coupling force acting at the coupling edge. The whole system is coupled by the distributed internal forces $[\mathbf{f}_{cp}] = [N_{yy}, Q_y, M_{yy}]^{\mathrm{T}}$, as shown in Fig. 2, acting along the coupling edges of the plate and $[\mathbf{f}_{cs}] = [N_{\theta\theta}, Q_\theta, M_{\theta\theta}]^{\mathrm{T}}$, as shown in Fig. 3, acting along the coupling edges of the shell.

2.1. Vibration of a substructure

As shown in Figs. 2 and 3, each subsystem is treated as an idealized system consisting of a single rectangular uniform plate or a uniform cylindrical shell. Their structural damping properties are represented by a linear Voigt viscoelastic model with hysteretic damping or loss factor η [39]. Under the assumption of thin shell theory [31], the differential equations describing the dynamic

behaviour of the cylindrical shell in the axial (x), tangential (θ) and radial (z) directions as shown in Fig. 3 are expressed as

$$\frac{\partial^2 u_x}{\partial x^2}+\frac{(1-\mu)}{2R^2}(1+\beta^2)\frac{\partial^2 u_x}{\partial \theta^2}+\frac{(1+\mu)}{2R}\frac{\partial^2 u_\theta}{\partial x\partial\theta}+\frac{\mu}{R}\frac{\partial u_z}{\partial x}-R\beta^2\frac{\partial^3 u_z}{\partial x^3}+\beta^2\frac{(1-\mu)}{2R}\frac{\partial^3 u_z}{\partial x\partial\theta^2}-\frac{\ddot{u}_x}{c_p^2}=-f_x\frac{(1-\mu^2)}{Eh_s}, \tag{1}$$

$$\frac{1+\mu}{2R}\frac{\partial^2 u_x}{\partial x\partial\theta}+\frac{(1-\mu)}{2}(1+3\beta^2)\frac{\partial^2 u_\theta}{\partial x^2}+\frac{\partial^2 u_\theta}{\partial\theta^2}+\frac{1}{R^2}\frac{\partial u_z}{\partial\theta}-\frac{(3-\mu)}{2}\beta^2\frac{\partial^3 u_z}{\partial x^2\partial\theta}-\frac{\ddot{u}_\theta}{c_p^2}=-f_\theta\frac{(1-\mu^2)}{Eh_s}, \tag{2}$$

$$\frac{\mu}{R}\frac{\partial u_x}{\partial x}-R\beta^2\frac{\partial^3 u_x}{\partial x^3}+\beta^2\frac{1-\mu}{2R}\frac{\partial^3 u_x}{\partial x\partial\theta^2}+\frac{1}{R^2}\frac{\partial u_\theta}{\partial\theta}-\frac{(3-\mu)}{2}\beta^2\frac{\partial^3 u_\theta}{\partial x^2\partial\theta}+(1+\beta)\frac{u_z}{R^2}+\beta^2\left(R^2\frac{\partial^4 u_z}{\partial x^4}+2\frac{\partial^4 u_z}{\partial x^2\partial\theta^2}+\frac{1}{R^2}\frac{\partial^4 u_z}{\partial\theta^4}\right)+2\beta^2\frac{\partial^2 u_z}{R^2\partial\theta^2}+\frac{\ddot{u}_z}{c_p^2}=f_z\frac{(1-\mu^2)}{Eh_s}, \tag{3}$$

with stress-displacement relations

$$N_{xx}=\frac{Eh_s}{(1-\mu^2)}\left[\frac{\partial u_x}{\partial x}+\mu\left(\frac{1}{R}\frac{\partial u_\theta}{\partial\theta}+\frac{u_z}{R}\right)\right]-\frac{D}{R}\frac{\partial^2 u_z}{\partial x^2},$$

$$N_{\theta\theta}=\frac{Eh_s}{(1-\mu^2)}\left[\frac{1}{R}\frac{\partial u_\theta}{\partial\theta}+\frac{u_z}{R}+\mu\frac{\partial u_x}{\partial x}\right]+\frac{D}{R^3}\frac{\partial^2 u_z}{\partial\theta^2},\ N_{x\theta}\approx N_{\theta x}\approx\frac{Eh_s}{2(1+\mu)}\left[\frac{1}{R}\frac{\partial u_x}{\partial\theta}+\frac{\partial u_\theta}{\partial x}\right], \tag{4}$$

$$M_{xx}=-D\left[\frac{\partial^2 u_z}{\partial x^2}+\frac{\mu}{R^2}\left(\frac{\partial^2 u_z}{\partial\theta^2}-\frac{\partial u_\theta}{\partial\theta}\right)-\frac{1}{R}\frac{\partial u_x}{\partial x}\right],\ M_{\theta\theta}=-D\left[\mu\frac{\partial^2 u_z}{\partial x^2}+\frac{1}{R^2}\left(\frac{\partial^2 u_x}{\partial\theta^2}+u_z\right)\right],$$

$$M_{x\theta}=M_{\theta x}=-D(1-\mu)\left[\frac{1}{R}\left(\frac{\partial^2 u_z}{\partial x\partial\theta}-\frac{\partial u_\theta}{\partial x}\right)\right], \tag{5}$$

$$Q_x=\frac{\partial M_x}{\partial x}+\frac{1}{R}\frac{\partial M_{\theta x}}{\partial\theta},\quad Q_\theta=\frac{1}{R}\frac{\partial M_\theta}{\partial\theta}+\frac{\partial M_{x\theta}}{\partial x}, \tag{6}$$

where $c_p=\sqrt{E/\rho(1-\mu^2)}$ denotes the phase velocity of the compressional wave travelling in the elastic shell, $\beta^2=h_s^2/12R^2$ and f_x,f_θ,f_z denote the distributed forces along x,θ,z directions respectively.

It is assumed that simply supported boundary conditions apply at the ends of the cylindrical shell, but the axial displacement is not zero. This is analogous to the axial movement allowed at an end of a simply supported beam (see, for example, Warburton [40]). Under the influence of harmonic excitation and modal analysis theory [37,41] it is assumed that

$$u_x=\sum_{i=1}^{n}\sum_{j=1}^{m}U_{ij}\cos j\theta\cos k_i x\,\mathrm{e}^{\mathrm{i}\omega t}, \tag{7}$$

$$u_\theta = \sum_{i=1}^{n} \sum_{j=1}^{m} V_{ij} \sin j\theta \sin k_i x \, e^{i\omega t}, \tag{8}$$

$$u_z = \sum_{i=1}^{n} \sum_{j=1}^{m} W_{ij} \cos j\theta \sin k_i x \, e^{i\omega t}, \tag{9}$$

where $k_i = i\pi/l$.

The substitution of Eqs. (7)–(9) into equations of motion (1)–(3) yields a homogeneous set of three linear algebraic equations for the displacement amplitudes U_{ij}, V_{ij}, W_{ij} given by

$$\begin{bmatrix} L_{11} & L_{12} & L_{13} \\ L_{21} & L_{22} & L_{23} \\ L_{31} & L_{32} & L_{33} \end{bmatrix} \begin{bmatrix} U_{ij} \\ V_{ij} \\ W_{ij} \end{bmatrix} = \begin{bmatrix} F_x \\ F_\theta \\ F_z \end{bmatrix}. \tag{10}$$

Here,

$$L_{11} = R^2 k_i^2 + \frac{1-\mu}{2}(1+\beta^2) j^2 - \lambda^2, \tag{11}$$

$$L_{12} = L_{21} = -\frac{1+\mu}{2} R j k_i, \tag{12}$$

$$L_{13} = L_{31} = -\mu R k_i - \frac{1-\mu}{2} R\beta^2 j^2 k_i + \beta^2 (k_i R)^3, \tag{13}$$

$$L_{22} = \frac{1-\mu}{2} R^2 (1+3\beta^2) k_i^2 + j^2 - \lambda^2, \tag{14}$$

$$L_{23} = L_{32} = \frac{3-\mu}{2} \beta^2 j (k_i R)^2 + j, \tag{15}$$

$$L_{33} = 1 + \beta^2 (R^2 k_i^2 + j^2)^2 - \beta^2 (2j^2 - 1) - \lambda^2, \tag{16}$$

where $\lambda = \omega R/c_p$ is a non-dimensional frequency, and

$$F_x = 2a^2 \frac{1-\mu^2}{E h_s l \pi} \int_0^l \int_0^{2\pi} f_x \cos j\theta \cos k_i x \, dx \, d\theta, \tag{17}$$

$$F_\theta = 2a^2 \frac{1-\mu^2}{E h_s l \pi} \int_0^l \int_0^{2\pi} f_\theta \sin j\theta \sin k_i x \, dx \, d\theta, \tag{18}$$

$$F_z = 2a^2 \frac{1-\mu^2}{E h_s l \pi} \int_0^l \int_0^{2\pi} f_z \cos j\theta \sin k_i x \, dx \, d\theta. \tag{19}$$

If a moment M_e is applied in the θ-direction at position (x_e, θ_e) on the shell, Eqs. (17)–(19) become

$$F_x = 0, \tag{20}$$

$$f_\theta = 2 \frac{(1-\mu^2)}{E h_s l \pi} M_e \sin j\theta_e \sin k_i x_e, \tag{21}$$

$$F_z = 2a\frac{(1-\mu^2)}{Eh_s l\pi}\int_0^{2\pi}\int_0^{l}\frac{\partial}{a\partial\theta}[M_e\delta(\theta-\theta_e)\delta(x-x_e)]\cos j\theta\sin k_i x\,\mathrm{d}x\,\mathrm{d}\theta$$
$$= -2\frac{(1-\mu^2)}{Eh_s l\pi}\int_0^{2\pi}\int_0^{l}\frac{\partial}{\partial\theta}[\cos j\theta\sin k_i x]M_e\delta(\theta-\theta_e)\delta(x-x_e)\,\mathrm{d}x\,\mathrm{d}\theta$$
$$= 2j\frac{(1-\mu^2)}{Eh_s l\pi}M_e\sin j\theta_e\sin k_i x_e. \tag{22}$$

It follows from these results that the response represented by Eqs. (7)–(9) of the cylindrical shell can be determined under any kind of excitation. The applied forces f_x, f_θ, f_z in Eqs. (1)–(3) consist of both external exciting forces and internal coupling forces. For this linear system, it is convenient to express the displacements U_{ij}, V_{ij}, W_{ij} described by Eqs. (7)–(10) in a summation form involving two components. Namely, the one induced by external exciting forces and the other by internal coupling forces. Therefore, the displacement and rotation angle $\{\mathbf{u}_{cs}^{(1)}\}, \{\mathbf{u}_{cs}^{(2)}\}$ of the shell at two coupling edges are represented in the summation form:

$$\begin{Bmatrix}\mathbf{u}_{cs}^{(1)}\\ \mathbf{u}_{cs}^{(2)}\end{Bmatrix} = \begin{bmatrix}\mathbf{R}_s^{11} & \mathbf{R}_s^{12}\\ \mathbf{R}_s^{21} & \mathbf{R}_s^{22}\end{bmatrix}\begin{Bmatrix}\mathbf{f}_{cs}^{(1)}\\ \mathbf{f}_{cs}^{(2)}\end{Bmatrix} + \begin{Bmatrix}\mathbf{R}_{es}^{1}\mathbf{f}_{es}\\ \mathbf{R}_{es}^{2}\mathbf{f}_{es}\end{Bmatrix}, \tag{23}$$

where $\mathbf{R}_s$ and $\mathbf{R}_{es}$ denote the interface receptance functions of the shell under internal coupling forces $\{\mathbf{f}_{cs}^{(1)}\}$, $\{\mathbf{f}_{cs}^{(2)}\}$ and external excitations $\{\mathbf{f}_{es}\}$ respectively. These receptance functions representing the displacement response vectors under each unit internal coupling force or external exciting force are determined using modal theory and Eq. (10). The internal coupling forces $\{\mathbf{f}_{cs}^{(1)}\}$, $\{\mathbf{f}_{cs}^{(2)}\}$ remain unknown and need to be determined by undertaking a synthesis process using geometrical compatibility conditions and force balance equations at the two coupling edges as described in Sections 2.2 and 2.3.

If it is assumed $R\to\infty$ and by changing the cylindrical co-ordinate system of Eqs. (1)–(3) to a Cartesian co-ordinate system then Eqs. (1) and (2) transform to differential equations describing the in-plane vibration of the plate substructure and Eq. (3) the differential equation describing its bending vibration. The stress–displacement relations of the plate substructure retain the same form as expressed in Eqs. (4)–(6).

Gorman [42], Leissa [43] developed a theoretical model to describe the free vibration of a uniform rectangular plate. After the natural frequencies ω_{rs} and principal modal shapes φ_{rs} of a uniform plate are determined, according to modal superposition theory, its response can be written as

$$u_x(x,y,t) = \sum_{r=1}\sum_{s=1}\varphi_{rs}^{Ix}(x,y)p_{rs}^{Ix}(t), \tag{24}$$

$$u_y(x,y,t) = \sum_{r=1}\sum_{s=1}\varphi_{rs}^{Iy}(x,y)p_{rs}^{Iy}(t), \tag{25}$$

$$u_z(x,y,t) = \sum_{r=1}\sum_{s=1}\varphi_{rs}^{b}(x,y)p_{rs}^{b}(t), \tag{26}$$

where φ_{rs}^{Ix}, φ_{rs}^{Iy} denote the modal shapes associated with the in-plane vibration of the plate in the x and y directions, respectively, whereas p_{rs}^{Ix}, p_{rs}^{Iy} represent their corresponding principal

co-ordinates. The terms φ_{rs}^{b}, p_{rs}^{b} designate the modal shapes and the principal co-ordinate of bending vibration of the rectangular plate and $1 \leqslant r \leqslant n$, $1 \leqslant s \leqslant m$ denote the number of modes admitted in the numerical scheme of the study.

The descriptions of displacement and rotation angle $\{\mathbf{u}_{cp}^{(1)}\}, \{\mathbf{u}_{cp}^{(2)}\}$ at the two coupling edges of the plate under internal coupling forces $\{\mathbf{f}_{cp}^{(1)}\}$, $\{\mathbf{f}_{cp}^{(2)}\}$ and external excitations $\{\mathbf{f}_{ep}\}$ have a similar matrix form to Eq. (23). That is,

$$\begin{Bmatrix} \mathbf{u}_{cp}^{(1)} \\ \mathbf{u}_{cp}^{(2)} \end{Bmatrix} = \begin{bmatrix} \mathbf{R}_p^{11} & \mathbf{R}_p^{12} \\ \mathbf{R}_p^{21} & \mathbf{R}_p^{22} \end{bmatrix} \begin{Bmatrix} \mathbf{f}_{cp}^{(1)} \\ \mathbf{f}_{cp}^{(2)} \end{Bmatrix} + \begin{Bmatrix} \mathbf{R}_{ep}^{1}\mathbf{f}_{ep} \\ \mathbf{R}_{ep}^{2}\mathbf{f}_{ep} \end{Bmatrix}. \tag{27}$$

2.2. Conservative coupling and synthesis of substructures

When the coupling edges of the plate and cylindrical shell are directly connected, the coupling conditions applying between the two substructures are described by their force balance and geometric compatible conditions acting at the coupling edges. In the global co-ordinate system, these conditions are expressed as follows:

$$\begin{Bmatrix} \mathbf{T}_p\mathbf{f}_{cp}^{(1)} \\ \mathbf{T}_p\mathbf{f}_{cp}^{(2)} \end{Bmatrix} + \begin{Bmatrix} \mathbf{T}_{s1}\mathbf{f}_{cs}^{(1)} \\ \mathbf{T}_{s2}\mathbf{f}_{cs}^{(2)} \end{Bmatrix} = \mathbf{0}, \tag{28}$$

$$\begin{Bmatrix} \mathbf{T}_p\mathbf{u}_{cp}^{(1)} \\ \mathbf{T}_p\mathbf{u}_{cp}^{(2)} \end{Bmatrix} + \begin{Bmatrix} \mathbf{T}_{s1}\mathbf{u}_{cs}^{(1)} \\ \mathbf{T}_{s2}\mathbf{u}_{cs}^{(2)} \end{Bmatrix}. \tag{29}$$

Here $\mathbf{T}_p$ denotes the transformation matrix from the plate local co-ordinate system to the global co-ordinate system, $\mathbf{T}_{s1}$, $\mathbf{T}_{s2}$ represent the transformation matrices from the local cylindrical co-ordinate system to the global co-ordinate system, defined at the two coupling edges respectively.

From Eq. (28) and by using the inverse transformation matrices the following result is obtained:

$$\begin{Bmatrix} \mathbf{f}_s^{(1)} \\ \mathbf{f}_s^{(2)} \end{Bmatrix} = -\begin{Bmatrix} \mathbf{T}_{s1}^{-1}\mathbf{T}_p\mathbf{f}_p^{(1)} \\ \mathbf{T}_{s2}^{-1}\mathbf{T}_p\mathbf{f}_p^{(2)} \end{Bmatrix}, \tag{30}$$

where the subscript c is neglected. The substitution of Eqs. (23), (27) and (30) into Eq. (29) allows the coupling relations to be expressed in the form

$$([\mathbf{R}_{pG}] + [\mathbf{R}_{sG}]) \begin{Bmatrix} \mathbf{T}_p\mathbf{f}_p^{(1)} \\ \mathbf{T}_p\mathbf{f}_p^{(2)} \end{Bmatrix} = \begin{Bmatrix} \mathbf{T}_{s1}\mathbf{R}_{se}^{1}\mathbf{f}_{se} \\ \mathbf{T}_{s2}\mathbf{R}_{se}^{2}\mathbf{f}_{se} \end{Bmatrix} - \begin{Bmatrix} \mathbf{T}_p\mathbf{R}_{pe}^{1}\mathbf{f}_{pe} \\ \mathbf{T}_p\mathbf{R}_{pe}^{2}\mathbf{f}_{pe} \end{Bmatrix}, \tag{31}$$

where

$$[\mathbf{R}_{pG}] = \begin{bmatrix} \mathbf{T}_p\mathbf{R}_p^{11}\mathbf{T}_p^{-1} & \mathbf{T}_p\mathbf{R}_p^{12}\mathbf{T}_p^{-1} \\ \mathbf{T}_p\mathbf{R}_p^{21}\mathbf{T}_p^{-1} & \mathbf{T}_p\mathbf{R}_p^{22}\mathbf{T}_p^{-1} \end{bmatrix}, \tag{32}$$

$$[\mathbf{R}_{sG}] = \begin{bmatrix} \mathbf{T}_{s1}\mathbf{R}_s^{11}\mathbf{T}_{s1}^{-1} & \mathbf{T}_{s1}\mathbf{R}_s^{12}\mathbf{T}_{s2}^{-1} \\ \mathbf{T}_{s2}\mathbf{R}_s^{21}\mathbf{T}_{s1}^{-1} & \mathbf{T}_{s2}\mathbf{R}_s^{22}\mathbf{T}_{s2}^{-1} \end{bmatrix}. \tag{33}$$

It therefore follows that the response of the whole system can be determined after derivation of solution of the receptance functions of the plate and the cylindrical shell.

2.3. Compliant-Dissipative Coupling and synthesis

In many engineering applications, two substructures are assumed connected by spring–damper systems. In general, these spring–damper systems can be treated as independent substructures. To simplify calculation, assume that the spring–damper systems between the plate and the shell are massless, the couplings between substructures are treated as compliant-dissipative and the spring–damper systems along the coupling edges have different constant complex stiffness coefficients in each displacement and rotational direction. This allows the complex stiffness matrix at any position along the coupling edge in the global co-ordinate system to be written as

$$[\mathbf{K}_D] = \begin{Bmatrix} K_Y(1+\mathrm{i}\eta_y) \\ K_Z(1+\mathrm{i}\eta_z) \\ K_\theta(1+\mathrm{i}\eta_\theta) \end{Bmatrix}. \tag{34}$$

The force balance conditions and responses of the substructures expressed in Eqs. (23), (27) and (28) remain unchanged. The geometrical compatibility equations at two coupling edges in the global co-ordinate system are now written as

$$\begin{Bmatrix} \mathbf{T}_p\mathbf{f}_{cp}^{(1)} \\ \mathbf{T}_p\mathbf{f}_{cp}^{(2)} \end{Bmatrix} = \begin{Bmatrix} [\mathbf{K}_D^{(1)}](\mathbf{T}_{s1}\mathbf{u}_{cs}^{(1)} - \mathbf{T}_p\mathbf{u}_{cp}^{(1)}) \\ [\mathbf{K}_D^{(2)}](\mathbf{T}_{s2}\mathbf{u}_{cs}^{(2)} - \mathbf{T}_p\mathbf{u}_{cp}^{(2)}) \end{Bmatrix} = -\begin{Bmatrix} \mathbf{T}_{s1}\mathbf{f}_{cs}^{(1)} \\ \mathbf{T}_{s2}\mathbf{f}_{cs}^{(2)} \end{Bmatrix}. \tag{35}$$

Substituting Eqs. (23) and (27) into Eq. (35), the coupling relations become

$$\begin{aligned} \begin{Bmatrix} \mathbf{T}_p\mathbf{f}_{cp}^{(1)} \\ \mathbf{T}_p\mathbf{f}_{cp}^{(2)} \end{Bmatrix} &= \begin{Bmatrix} [\mathbf{K}_D^{(1)}](-\mathbf{T}_{s1}\mathbf{R}_s^{11}\mathbf{T}_{s1}^{-1}\mathbf{T}_p\mathbf{f}_{cp}^{(1)} - \mathbf{T}_{s1}\mathbf{R}_s^{12}\mathbf{T}_{s2}^{-1}\mathbf{T}_p\mathbf{f}_{cp}^{(2)} + \mathbf{T}_{s1}\mathbf{R}_{es}^{1}\mathbf{f}_{es} \\ \quad - \mathbf{T}_p\mathbf{R}_p^{11}\mathbf{T}_p^{-1}\mathbf{T}_p\mathbf{f}_{cp}^{(1)} - \mathbf{T}_p\mathbf{R}_p^{12}\mathbf{T}_p^{-1}\mathbf{T}_p\mathbf{f}_{cp}^{(2)} - \mathbf{T}_p\mathbf{R}_{ep}^{1}\mathbf{f}_{ep}) \\ [\mathbf{K}_D^{(2)}](\mathbf{T}_{s2}\mathbf{R}_s^{21}\mathbf{T}_{s1}^{-1}\mathbf{f}_{cp}^{(2)} - \mathbf{T}_{s2}\mathbf{R}_s^{22}\mathbf{T}_{s2}^{-1}\mathbf{T}_p\mathbf{f}_{cp}^{(2)} + \mathbf{T}_{s2}\mathbf{R}_{es}^{2}\mathbf{f}_{es} \\ \quad - \mathbf{T}_p\mathbf{R}_p^{21}\mathbf{T}_p^{-1}\mathbf{T}_p\mathbf{f}_{cp}^{(1)} - \mathbf{T}_p\mathbf{R}_p^{22}\mathbf{T}_p^{-1}\mathbf{T}_p\mathbf{f}_{cp}^{(2)} - \mathbf{T}_p\mathbf{R}_{ep}^{2}\mathbf{f}_{ep}) \end{Bmatrix} \\ &= -[\mathbf{K}_D]\left(([\mathbf{R}_{sG}] + [\mathbf{R}_{pG}])\begin{Bmatrix} \mathbf{T}_p\mathbf{f}_{cp}^{(1)} \\ \mathbf{T}_p\mathbf{f}_{cp}^{(2)} \end{Bmatrix} + \begin{Bmatrix} \mathbf{T}_{s1}\mathbf{R}_{es}^{1}\mathbf{f}_{es} \\ \mathbf{T}_{s2}\mathbf{R}_{es}^{2}\mathbf{f}_{es} \end{Bmatrix} - \begin{Bmatrix} \mathbf{T}_p\mathbf{R}_{ep}^{1}\mathbf{f}_{ep} \\ \mathbf{T}_pR_{ep}^{2}\mathbf{f}_{ep} \end{Bmatrix}\right), \end{aligned} \tag{36}$$

where

$$[\mathbf{K}_D] = \begin{bmatrix} \mathbf{K}_D^{(1)} & \mathbf{0} \\ \mathbf{0} & \mathbf{K}_D^{(2)} \end{bmatrix}. \tag{37}$$

Therefore, the coupling forces in the global co-ordinate system may be expressed as

$$\begin{Bmatrix} \mathbf{T}_p\mathbf{f}_{cp}^{(1)} \\ \mathbf{T}_p\mathbf{f}_{cp}^{(2)} \end{Bmatrix} = ([\mathbf{I}] + [\mathbf{K}_D][\mathbf{R}_{pG}] + [\mathbf{K}_D][\mathbf{R}_{sG}])^{-1}[\mathbf{K}_D]\left(\begin{Bmatrix} \mathbf{T}_{s1}\mathbf{R}_{es}^{1}\mathbf{f}_{es} \\ \mathbf{T}_{s2}\mathbf{R}_{es}^{2}\mathbf{f}_{es} \end{Bmatrix} - \begin{Bmatrix} \mathbf{T}_p\mathbf{R}_{ep}^{1}\mathbf{f}_{ep} \\ \mathbf{T}_p\mathbf{R}_{ep}^{2}\mathbf{f}_{ep} \end{Bmatrix}\right). \tag{38}$$

3. Power flow characteristics in a plate–cylindrical shell system

3.1. Power flow density vector

Xing and Price [23] expressed and discussed the basic definition of a power flow density vector in a continuum. Using this definition, the instantaneous power flow density vector in a thin plate is defined in the form

$$q_k = -\mathrm{Re}\{\dot{u}_z\}\mathrm{Re}\{Q_k\} + \mathrm{Re}\{\dot{u}_{z,j}\}\mathrm{Re}\{M_{jk}\} - \mathrm{Re}\{\dot{u}_j\}\mathrm{Re}\{N_{jk}\}, \tag{39}$$

with a time-averaged quantity

$$\langle q_k \rangle = -\tfrac{1}{2}\mathrm{Re}\{Q_k\dot{u}_z^* - M_{kj}\dot{u}_{z,j}^* + N_{kj}\dot{u}_k^*\}, \tag{40}$$

where $j = 1, 2 = k$. In these equations a standard Cartesian tensor notation and a summation convention are used. The sign of the second term on the right-hand side of Eqs. (39) and (40) is dependent on the direction definitions of $\dot{\theta}_j$ and M_{jk}. These definitions are based on the sign convention of elasticity theory (see, for example, Reismann and Pawlik [44]).

The time-averaged power flow density vector $\langle q_k \rangle$ in Eq. (40) is equivalent to a structural intensity parameter [20,21] and has similarity to an acoustic intensity parameter in a fluid domain being the product of pressure and the in-phase component of fluid particle velocity (see, for example, [45]).

Similarly, the instantaneous power flow density vector in a thin shell is given by

$$q_k = -\mathrm{Re}\{\dot{u}_z\}\mathrm{Re}\{Q_k\} + \mathrm{Re}\{\dot{u}_{z,j} - \dot{u}_k/R_k\}\mathrm{Re}\{M_{jk}\} - \mathrm{Re}\{\dot{u}_j\}\mathrm{Re}\{N_{jk}\}, \tag{41}$$

with a time-averaged quantity

$$\langle q_k \rangle = -\tfrac{1}{2}\mathrm{Re}\{Q_k\dot{u}_z^* - M_{kj}(\dot{u}_{z,j}^* - \dot{u}_k^*/R_k) + N_{kj}\dot{u}_k^*\}, \tag{42}$$

where R_k is the radius of the shell curvature about the k-axis. Here, for a thin cylindrical shell, $R_1 = R, R_2 = \infty$.

The instantaneous power flow density vector across one coupling edge is only in the y direction of the plate (see, Fig. 2) and can be expressed as

$$\begin{aligned} q_y^c = &-\mathrm{Re}\{\dot{u}_z\}\mathrm{Re}\{Q_y\} + \mathrm{Re}\{\dot{\boldsymbol{\theta}}_y\}\mathrm{Re}\{M_{xy}\} + \mathrm{Re}\{\dot{\boldsymbol{\theta}}_x\}\mathrm{Re}\{M_{yy}\} \\ &- \mathrm{Re}\{\dot{u}_x\}\mathrm{Re}\{N_{xy}\} - \mathrm{Re}\{\dot{u}_y\}\mathrm{Re}\{N_{yy}\}. \end{aligned} \tag{43}$$

The total transmitted power at a coupling edge is given by the integral of the transmitted power flow density along the length of the coupling edge. That is,

$$q_{trans} = \int_0^a q_y^c \mathrm{d}x, \tag{44}$$

with the corresponding time-averaged quantity

$$\langle q_{trans} \rangle = \int_0^a \langle q_y^c \rangle \, \mathrm{d}x. \tag{45}$$

It is convenient to determine the power flow at the coupling edge using a substructure receptance approach because the solution of the coupling force in the coupling relationship

described in Eqs. (30), (31) and the receptance function expressed in Eq. (27) are simple and in the same local co-ordinate axis system.

3.2. Calculation example

For illustrative purposes, assume that the plate–cylindrical shell system shown in Fig. 1 is defined by the data set: $\rho = 7750$ kg/m^3, $E = 206$ GPa, $\eta = 0.01$, $\mu = 0.3$; $R = 0.177$ m, $a = l = 1.284$ m, $h_p = 0.003$ m, $h_s = 0.005$ m; and the angles of the two coupling edges in the cylindrical co-ordinate system are given as $\theta_{b1} = -\theta_{b2} = 60^\circ$.

Two coupling edge conditions were examined. The first case assumes that the plate and the cylindrical shell are directly connected at the coupling edges. This implies that the coupling is conservative, all power output from the source substructure inputs to the receiver substructure. The second case assumes that they are connected by uniform distributed spring–dampers at the coupling edges. Therefore, the coupling is compliant and dissipative and a portion of the power output from the source substructure stores and dissipates in the coupling spring–dampers.

3.2.1. Conservative coupling

Figs. 4 and 5 illustrate the variation of the time-averaged input power of external excitation and total transmitted power flow along two coupling edges from the plate to the shell as a function of frequency. A unit amplitude loading is applied at the centre of the plate. The results derived by a FEA model are included to verify the substructure calculations.

The FEA model consists of 1209 nodes (341 nodes for the plate and 930 nodes for the shell) and 1200 plate–shell elements. In the calculation, 150 natural frequencies and principal modes of the system were extracted using FEA package ANSYS spanning the frequency range up to 2200 Hz. The structural damping loss factor η of the plate and the shell are used in the mode equations to derive the displacement response from the FEA calculation. From the node deflections of an element, the spatial averaged squared surface velocity of this element was derived to calculate the transmitted power flow using Eq. (46). Since the receiver shell is not connected to any other

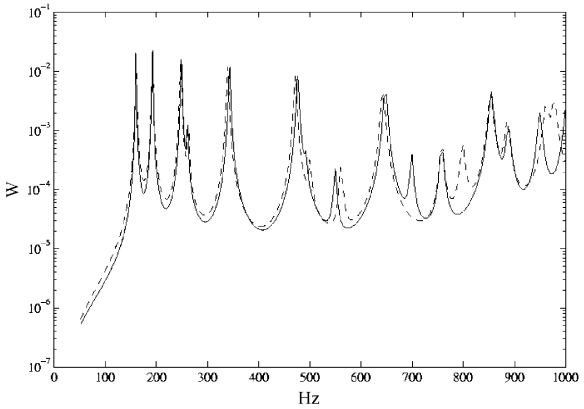

Fig. 4. Predictions of time-averaged input power flow of external excitation (excitation at the centre of the plate); ——, input power, – – –, input power (FEA).

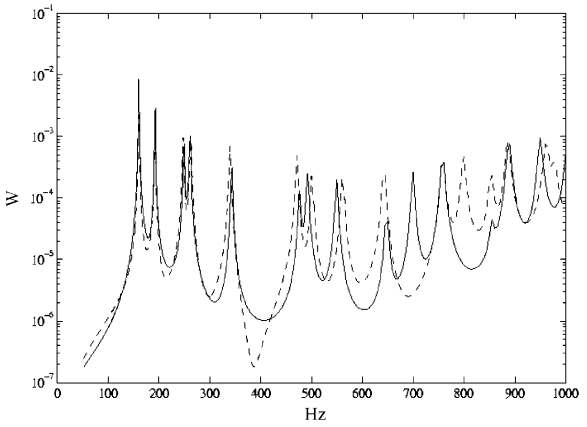

Fig. 5. Predictions of time-averaged transmitted power flow from the plate to the shell (excitation at the centre of the plate); ——, transmitted power, – – –, transmitted power (FEA).

substructure except the source plate, the transmitted time-averaged power determined by the FEA model approximately equals the rate of energy dissipation of the shell due to the internal loss factor (see, [39]). This comparison is illustrated in Fig. 5 since

$$\langle q_{trans} \rangle \approx \omega\eta\rho\pi Rlh_s\overline{|v_s^2(f)|} \approx \langle q_{in} \rangle - \omega\eta\rho abh_p\overline{|v_p^2(f)|}, \tag{46}$$

where $\overline{|v_s^2(f)|}$, $\overline{|v_p^2(f)|}$ denote spatial average squared velocities of the shell and plate respectively. The total energy dissipation of the system in a vibration period is equal to the time-averaged input power as shown in Fig. 4.

It is seen from Figs. 4 and 5 that except for small discrepancies in the natural frequency values, only small differences exist in the determination of the time-averaged input power of external excitation between the theoretical substructure predictions and those evaluated by the FEA approach, thus providing a measure of confidence in the validity of the computations. The reason for the errors occurring in the natural frequencies lies in the fact that different plate–shell theories are used in the two calculations. That is, the influences of transverse shear deformation and rotational inertia of a plate–shell element are incorporated into the ANSYS calculations but they are ignored in the theoretical model. In previous studies [32,34] relating to free vibration of a cylindrical shell with an internal floor, it was found that errors also occurred in the prediction of natural frequencies of some modes between theoretical methods and the FEA approach. As shown in Fig. 5, some errors are observed in the transmitted power flow from the plate to the shell, because an approximation (i.e. Eq. (46)) is used to calculate the transmitted power flow in the FEA model.

In the following presentation of spatial distributions of time-averaged power flow density vectors, Figs. 6 and 7 relate to a unit amplitude exciting force applied at position $x_e = 0.45$ m, $y_e = -0.023$ m indicated by the symbol "+" and defined in the local co-ordinate axes of the plate. For clarity of presentation, the modulus of time-averaged power flow density vectors in Figs. 6 and 7 are defined as

$$|\langle q(x,y)\rangle|^{(d)} = |\langle q(x,y)\rangle|^{0.2} = (|q_x(x,y)|^2 + |q_y(x,y)|^2)^{0.1}. \tag{47}$$

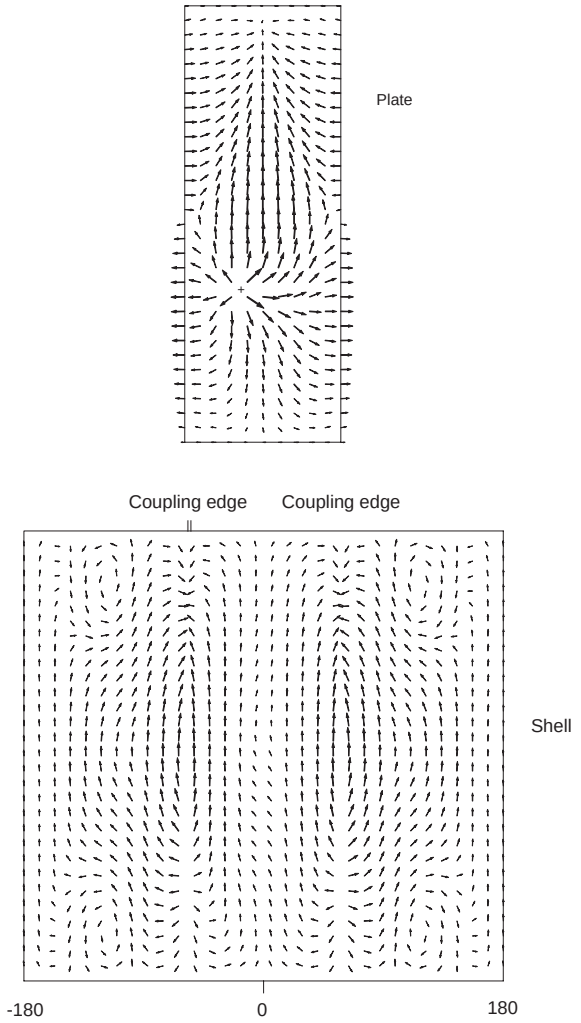

Fig. 6. Time-averaged input power flow density vector in the system, $f = 160.5$ Hz. "+" indicates the excitation position.

Fig. 6 illustrates the spatial distribution of the time-averaged power flow density vector at a frequency of 160.5 Hz. This corresponds to the first natural frequency of the system. Fig. 7 shows similar data corresponding to a frequency of 177 Hz which coincides with the second natural frequency of the system.

The power flow density vector displaying the dynamic behaviour of a plate–cylindrical shell under a single force excitation is very complex and frequency dependent in character. The power flow density at a position near to the source is not necessarily always larger than its density at positions further away from the source. Power flows from the excitation source and usually terminates at a boundary. Figs. 6 and 7 illustrate the possibility that the time-averaged power flow density is equal to zero at positions within the plate and a circulation or vortex type flow is

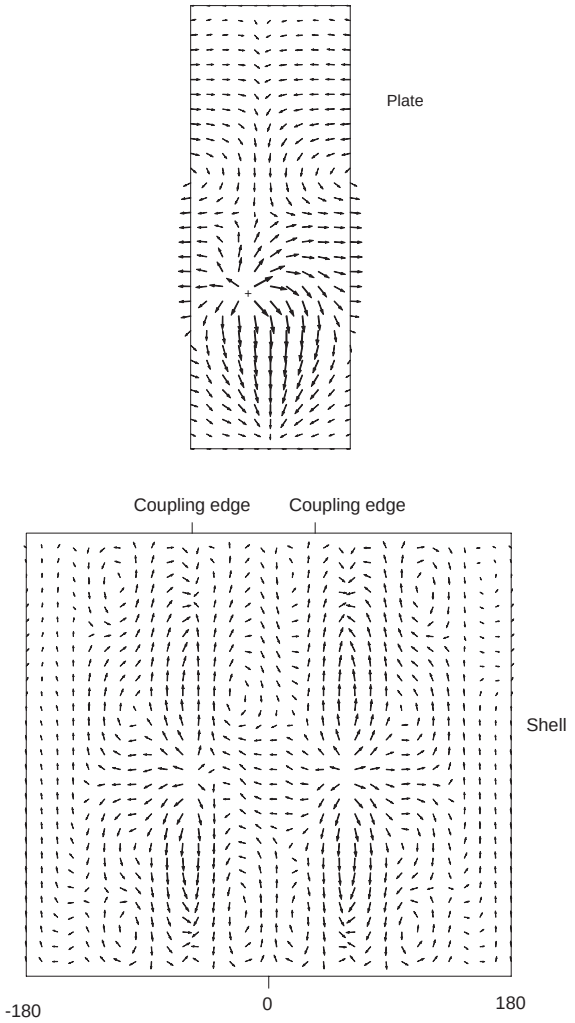

Fig. 7. Time-averaged input power flow density vector in the system, $f = 177.0$ Hz. "+" indicates the excitation position.

observed in the vicinity of this position. This behaviour further demonstrates that a heat conduction analogy [46] for mechanical power flow is not true [23].

One difficulty encountered in a general FEA modal superposition approach is the accuracy of predicting internal forces. Compared to the prediction of the displacement response, the calculation of the internal force exhibits slow or poor convergence and therefore a large number of modes is required for accurate predictions of energy flow which is a product of force and velocity. In the theoretical substructure approach adopted herein, the modes of the plate and the shell are defined by trigonometric or hyperbolic functions which have continuous derivatives, and therefore such difficulties can be overcome. The highest natural frequency admitted in the present calculation for a suitable accuracy of convergence of solution is at least 300 kHz.

3.2.2. Compliant and dissipative coupling

Fig. 8 schematically illustrates a section of a plate–cylindrical shell system with a compliant and dissipative coupling. The material and geometric properties of the plate and shell are the same as defined in the original model but a uniform distributed damper connects them. The complex stiffness per unit length of the damper is only in the z direction and defined by

$$K_D = 10^4(1 + i\eta_z)\,\mathrm{N/m^2}. \tag{48}$$

Figs. 9–11 illustrate the variation of the time-averaged power flow with frequency to different assumed coupling damping coefficient η_z. A unit force excitation is applied at the centre of the plate. Fig. 9 shows the results of time-averaged input power caused by the external excitation whereas Figs. 10 and 11 display the results of total time-averaged output power along two coupling edges from the plate and total input power to the shell respectively.

These figures illustrate that for different coupling damping models, the principal dynamic characteristics of the system remain nearly the same as measured by the natural frequencies of the system, the input power caused by the external excitation and the power from the damping coupling into the receiver shell. However, large differences are observed in the time-averaged power flowing from the plate to the dampers. This implies that the coupling dampers mainly absorb and dissipate the energy stored originally in the source plate because the total input power induced by external excitation must balance the total power dissipated in the plate, the shell and the dampers. There is no obvious influence caused by the coupling damping to the dynamic behaviour of the receiver shell and the time-averaged input power from the external excitation. Therefore, the bigger the coupling damping the larger the energy dissipation in the coupling damper system, thus reducing the energy dissipated in the plate.

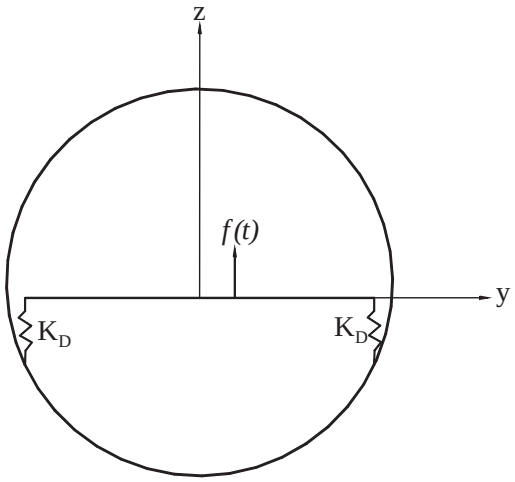

Fig. 8. Schematic illustration of a cross-section of a plate–cylindrical shell system with a compliant and dissipative coupling.

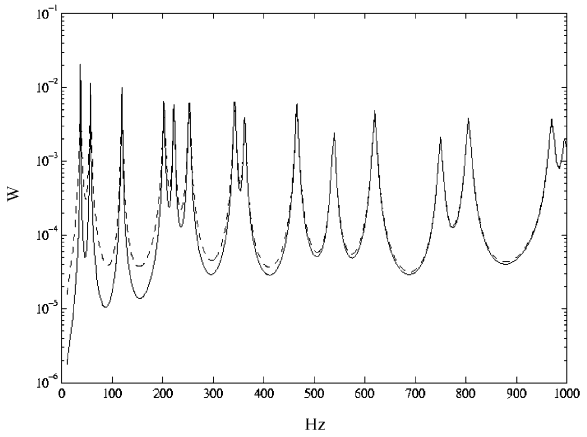

Fig. 9. Predictions of time-averaged input power flow for the compliant and dissipative coupling; ——, $\eta_z = 0.01$, – – –, $\eta_z = 0.1$.

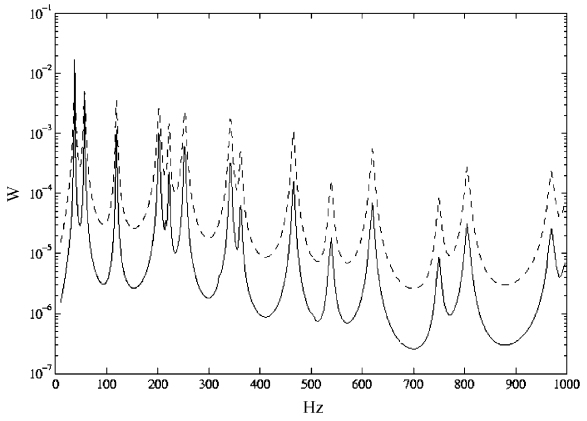

Fig. 10. Predictions of time-averaged output power flow from the plate for the compliant and dissipative coupling; ——, $\eta_z = 0.01$, – – –, $\eta_z = 0.1$.

4. Conclusion

In this paper, a receptance substructure approach is applied to investigate the power flow characteristics of a complex plate–cylindrical shell system. The receptance function of each substructure is formulated using theoretical descriptions of the modal shape functions. The displacement components induced by external forces and the interface coupling forces are deduced, permitting determination of the coupling forces and power flow between the interface of substructures by synthesizing through the force balance and geometric compatibility conditions applied at the coupled edges. Both conservative and dissipative couplings along the coupling edge are investigated. The power flow characteristics of the system are examined numerically. The proposed method calculates the higher modes easily and efficiently to ensure convergence of solution because the theoretically defined modes and internal forces are described by trigonometric or hyperbolic functions which have continuous derivatives.

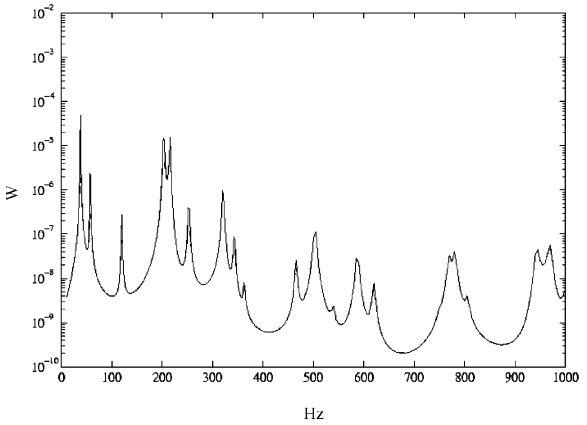

Fig. 11. Predictions of time-averaged transmitted power flow to the shell for the compliant and dissipative coupling; ——, $\eta_z = 0.01$, – – –, $\eta_z = 0.1$.

The power flow density vector associated with the plate–cylindrical shell displays complexity of form and is frequency dependent. The time-averaged power flow density value at positions near the source is not necessarily larger than its value at positions far from the source. Time-averaged power usually flows from the excitation source and ends at a boundary, but there is every likelihood that the time-averaged power flow density is equal to zero at positions within the plate, and a circulation or vortex like structure may exist around this zero density power flow position. This phenomenon implies that a heat conduction analogy for mechanical power flows is not true.

The main contribution of the coupling damping value in the compliant and dissipative coupling edge is observed in the power flowing to the source substructure plate. For the same applied excitation, the larger the coupling damping value, the greater the energy dissipation at the coupling edges with corresponding reduction of energy dissipated in the source plate.

Appendix A. Nomenclature

a, b	length and width of rectangular plate
D	flexural rigidity of plate or shell
E	Young's modulus
$f(t)$	general expression of exciting forces
$\mathbf{f}_c$	internal coupling force matrix
$\mathbf{f}_e$	external excitation force matrix
h_p, h_s	thickness of plate and shell
i	$= \sqrt{-1}$
m_{rs}	generalized modal mass
$M_{xx}, M_{yy}, M_{\theta\theta}$	internal bending moments and twisting moment per unit length
$M_{xy}, M_{x\theta}$	internal twisting moment per unit length
$[\mathbf{R}_e], [\mathbf{R}_c]$,	receptance functions between displacements at coupling edges and external excitations or internal coupling forces

n	mode number used in modal analysis
$N_{xx}, N_{yy}, N_{\theta\theta}$	extension force per unit length
$N_{xy}N_{x\theta}$	in-plane shear force per unit length
$p_{rs}(t)$	principal co-ordinate
Q_x, Q_y, Q_θ	transverse shearing forces per unit length
q	general expression for power flow
$\langle q \rangle$	general expression for time-averaged power flow
R	radius of cylindrical shell
T	a period of excitation
[**T**]	orthogonal transformation matrix between global and local co-ordinate systems
$u(t)$	general expression for displacement
u_x, u_θ, u_z	displacement components for shell shown in Fig. 3
u_x, u_y, u_z	displacement components for plate
U_{ij}, V_{ij}, W_{ij}	displacement amplitudes of mode ij of shell
x, y, z	spatial co-ordinates
α	the angle between global and local co-ordinate systems
η	damping loss factor
μ	Poisson ratio
θ	general expression for slope angle
θ_b	angle at the coupling edges in the cylindrical co-ordinate system
ρ	mass density
σ_{ij}	stress tensor
φ_r, φ_{rs}	principal mode shape
ω	exciting frequency
ω_{rs}	natural frequency
$[\,]^{\mathrm{T}}$	transpose of a matrix
$[\,]^{-1}$	an inverse matrix
$(*)$	conjugate of a complex variable

References

[1] H.G.D. Goyder, R.G. White, Vibrational power flow from machines into built-up structures. Part I. Introduction and approximate analyses of beam and plate-like foundations, *Journal of Sound and Vibration* 68 (1) (1980) 59–75.
[2] H.G.D. Goyder, R.G. White, Vibrational power flow from machines into built-up structures. Part II. Wave propagation and power flow in beam-stiffened plates, *Journal of Sound and Vibration* 68 (1) (1980) 77–95.
[3] H.G.D. Goyder, R.G. White, Vibrational power flow from machines into built-up structures. Part III. Power flow through isolation systems, *Journal of Sound and Vibration* 68 (1) (1980) 97–117.
[4] J.M. Cuschieri, Structural power-flow analysis using a mobility approach to a L-shape plate, *Journal of the Acoustical Society of America* 87 (1990) 1159–1165.
[5] R.S. Langley, Application of the dynamic stiffness method to the free and forced vibrations of aircraft panels, *Journal of Sound and Vibration* 135 (2) (1989) 319–331.
[6] D.W. Miller, A. von Flotow, A travelling wave approach to power flow in structural networks, *Journal of Sound and Vibration* 128 (1) (1989) 145–162.
[7] J.L. Horner, R.G. White, Prediction of vibration power transmission through bends and joints in beam-like structures, *Journal of Sound and Vibration* 147 (1) (1991) 87–103.

[8] L.S. Beale, M.L. Accorsi, Power flow in two and three dimensional frame structures, *Journal of Sound and Vibration* 185 (4) (1995) 685–702.
[9] Y.P. Xiong, J.T. Xing, W.G. Price, Power flow analysis of complex coupled systems by progressive approaches, *Journal of Sound and Vibration* 239 (2) (2001) 275–295.
[10] Z.H. Wang, J.T. Xing, W.G. Price, Power flow analysis of indeterminate rod/beam systems using a substructure method, *Journal of Sound and Vibration* 249 (1) (2002) 3–22.
[11] H. Farag, J. Pan, On the free and forced vibration of single and coupled rectangular plates, *Journal of the Acoustical Society of America* 104 (1) (1998) 204–216.
[12] M. Beshara, A.J. Keane, Vibrational energy flows between plates with compliant and dissipative couplings, *Journal of Sound and Vibration* 213 (3) (1998) 511–535.
[13] C. Simmons, Structure-borne sound transmission through plate junctions and estimates of SEA coupling loss factors using the FE method, *Journal of Sound and Vibration* 144 (1991) 215–227.
[14] G. Stimpson, N. Lalor, SEA extension of a FE model to predict total engine noise, *Internoise* 92 (1992) 557–560.
[15] J.A. Steel, R.J.M. Craik, Statistical energy analysis of structure-borne sound transmission by finite element methods, *Journal of Sound and Vibration* 178 (1993) 553–561.
[16] C.R. Fredo, A SEA-like approach for the derivation of energy flow coefficients with a finite element model, *Journal of Sound and Vibration* 199 (1992) 645–666.
[17] B.R. Mace, P.J. Shorter, Energy flow models from finite element analysis, *Journal of Sound and Vibration* 233 (3) (2000) 369–389.
[18] K. Shankar, A.J. Keane, Energy flow predictions in a structure of rigidly joined beams using receptance theory, *Journal of Sound and Vibration* 185 (1995) 867–890.
[19] K. Shankar, A.J. Keane, Vibrational energy flow analysis using a substructure approach: the application of receptance theory to FEA and SEA, *Journal of Sound and Vibration* 201 (1997) 491–513.
[20] S.A. Hambric, Power flow and mechanical intensity calculations in structural finite element analysis, *Journal of Vibration and Acoustical* 112 (1990) 542–549.
[21] L. Gavic, G. Pavic, A finite element method for computation of structural intensity by the normal mode approach, *Journal of Vibration and Acoustics* 164 (1993) 29–43.
[22] Z.H. Wang, J.T. Xing, W.G. Price, An investigation of power flow characteristics of L-shaped plates adopting a substructure approach, *Journal of Sound and Vibration* 250 (4) (2002) 627–648.
[23] J.T. Xing, W.G. Price, A power-flow analysis based on continuum dynamics, *Proceedings of the Royal Society A* 455 (1999) 401–436.
[24] J.T. Xing , W.G. Price, Z.H. Wang, A study of power flow characteristics using a vector field analysis approach, in: H. Hu (Editor-in-chief), *Proceedings of the Fifth International Conference on Vibration Engineering*, China Aviation Industry Press, Beijing, 2002, pp. 33–40.
[25] P.A. Franken, Input impedances of simple cylindrical structures, *Journal of the Acoustical Society of America* 32 (1960) 473–477.
[26] M. Heckl, Vibrations of point-driven cylindrical shell, *Journal of the Acoustical Society of America* 34 (1962) 1553–1557.
[27] C.R. Fuller, The input mobility of an infinite circular elastic shell with fluid, *Journal of Sound and Vibration* 87 (3) (1983) 409–427.
[28] A. Harari, Wave propagation in cylindrical shells with finite regions of structural discontinuity, *Journal of the Acoustical Society of America* 62 (1977) 1196–1205.
[29] R.S. Ming, J. Pan, M.P. Norton, The mobility functions and their application in calculating power flow in coupled cylindrical shells, *Journal of the Acoustical Society of America* 105 (1999) 1702–1713.
[30] W. Flugge, *Stresses in Shells*, Springer, New York, 1973.
[31] A.W. Leissa, Vibration of Shells, NASA SP-288, Washington, DC, 1973.
[32] M.R. Peterson, D.E. Boyd, Free vibration of circular cylinders with longitudinal interior partitions, *Journal of Sound and Vibration* 60 (1978) 45–62.
[33] R.S. Langley, A dynamic stiffness technique for the vibration analysis of stiffened shell structures, *Journal of Sound and Vibration* 156 (1992) 521–540.

[34] J. Missaoui, L. Cheng, M.J. Richard, Free and forced vibration of a cylindrical shell with a floor partition, *Journal of Sound and Vibration* 190 (1) (1996) 21–40.
[35] J. Missaoui, L. Cheng, Vibroacoustic analysis of a finite cylindrical shell with internal floor partition, *Journal of Sound and Vibration* 226 (1) (1999) 101–123.
[36] D.S. Li, L. Cheng, C.M. Gosselin, Analysis of structural acoustic coupling of a cylindrical shell with an internal floor partition, *Journal of Sound and Vibration* 250 (5) (2002) 903–921.
[37] R.E.D. Bishop, D.C. Johnson, *The Mechanics of Vibration*, Cambridge University Press, Cambridge, 1960.
[38] S.P. Timoshenko, S. Woinowsky-Krieger, *Theory of Plates and Shells*, 2nd Edition, McGraw-Hill, New York, 1959.
[39] L. Cremer, M. Heckl, E.E. Ungar, *Structure-borne Sound*, Springer, Berlin, 1988.
[40] G.B. Warburton, *The Dynamic Behaviour of Structures*, Pergamon Press, New York, 1976.
[41] Lord Rayleigh, *Theory of Sound*, Macmillan, London, 1894.
[42] D.J. Gorman, *Free Vibration Analysis of Rectangular Plates*, Elsevier, New York, 1982.
[43] A. Leissa, *Vibration of Plates*, Acoustical Society of America, Woodbury, NY, 1993.
[44] H. Reismann, P.S. Pawlik, *Elasticity Theory and Application*, Quantum, New York, 1980.
[45] F.J. Fahy, *Sound Intensity*, Elsevier Science Publishers, London, 1989.
[46] D.J. Nefske, S.H. Sung, Power flow element analysis of dynamic system: basic theory and application to beam, in: K.H. Hsu, D.J. Nefske, A. Akay (Eds.), *Statistical Energy Analysis* NCA-3, ASME, New York, 1987, pp. 47–54.